Low-threshold Raman laser from an on-chip, high-Q, polymer-coated microcavity

Bei-Bei Li,[1] Yun-Feng Xiao,[1,*] Meng-Yuan Yan,[1] William R. Clements,[1,2] and Qihuang Gong[1,3]

[1]*State Key Laboratory for Mesoscopic Physics & Department of Physics, Peking University, Beijing 100871, China*

[2]*Département de physique, École polytechnique, Palaiseau 91128, France*

[3]*e-mail: qhgong@pku.edu.cn*

**Corresponding author: yfxiao@pku.edu.cn*

Received March 25, 2013; revised April 23, 2013; accepted April 23, 2013;
posted April 23, 2013 (Doc. ID 187743); published May 20, 2013

We study the stimulated Raman emission of a high-Q polydimethylsiloxane (PDMS)-coated silica microsphere on a silicon chip. In this hybrid structure, as the thickness of the PDMS coating increases, the spatial distribution of the whispering gallery modes moves inside the PDMS layer, and the light emission switches from silica Raman lasing to PDMS Raman lasing. The Raman shift of the PDMS Raman laser is measured at 2900 cm^{-1}, corresponding to the strongest Raman fingerprint of bulk PDMS material. The threshold for this PDMS Raman lasing is demonstrated to be as low as 1.3 mW. This type of Raman emission from a surface-coated high-Q microcavity not only provides a route for extending lasing wavelengths, but also shows potential for detecting specific analytes.

OCIS codes: (140.3948) Microcavity devices; (290.5910) Scattering, stimulated Raman; (160.5470) Polymers; (190.4710) Optical nonlinearities in organic materials.

http://dx.doi.org/10.1364/OL.38.001802

Stimulated Raman scattering [1] requires very high pump power because of the extremely low Raman gain coefficient. Over the past few years, whispering-gallery-mode (WGM) microcavities [2,3] have shown potential for overcoming this problem, because they not only possess ultrahigh quality factors but also small mode volumes, and can therefore significantly enhance light–matter interactions. In other words, since both the excitation light and the emitted Raman laser are on resonance with the respective high-Q WGMs, the Raman lasing threshold, which is inversely proportional to the product of the Q factors of the excitation mode and Raman lasing mode can be decreased by several orders of magnitude. So far, liquid droplet microspheres [4,5], silicon [6], and silica [2,3] microcavity Raman lasers were demonstrated experimentally to possess low thresholds. On the other hand, due to low cost, good biocompatibility, large nonlinearity, and ease of doping, polymer-based microcavities have also attracted increasing interest [7–16]. However, polymer microcavity Raman lasers have not been reported so far. Generally, polymer materials have larger Raman shifts than inorganic materials (usually of the order of several hundred cm^{-1}), so can be used for further extending the wavelength range of lasers. For example, polydimethylsiloxane (PDMS) has its strongest Raman fingerprint at 2900 cm^{-1}, and the two strongest Raman peaks of polystyrene are 1000 cm^{-1} and 3058 cm^{-1}.

In this work, we fabricate PDMS-coated silica microsphere cavities on a silicon chip, in which the intrinsic quality factors of the WGMs exceed 10 million, limited by the PDMS material absorption in the 680 nm wavelength band. Note that we use a microsphere instead of a microtoroid because a microsphere supports more high-Q modes in one free spectral range than a microtoroid, thus ensuring that the wavelength region with high Raman gain overlaps with at least one of the WGMs. In our experiment, for a given pump power at which Raman emission is always present, when the coating thickness is gradually increased from zero to several micrometers, the emission spectrum exhibits a transition from silica Raman to PDMS Raman lasing. We demonstrate a pump threshold for pure PDMS Raman lasing as low as 1.3 mW.

The fabrication technique of the PDMS-coated silica microsphere on a silicon wafer [17,18] is shown in Fig. 1

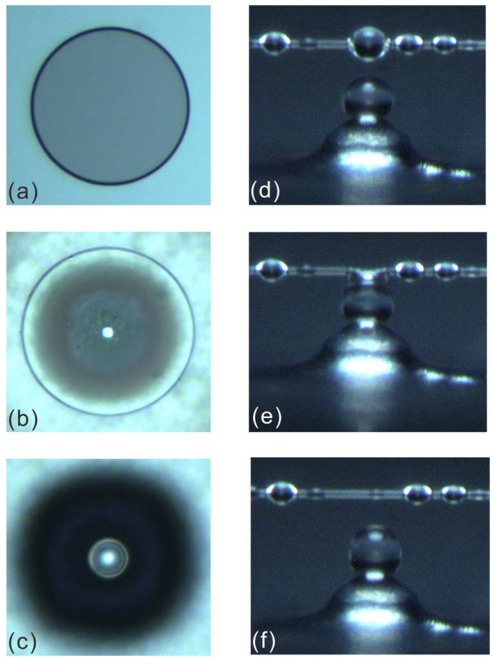

Fig. 1. Fabrication process of a PDMS-coated silica microsphere on a silicon wafer. (a) Top view optical image of a circular silica pad after lithography and hydrofluoric acid etching of silica. (b) Top view optical image of an undercut microdisk with a very thin supporting silicon pillar. (c) Top view optical image of an on-chip microsphere formed after CO_2 laser reflow. (d) Side view optical image of a microsphere (before coating) under PDMS droplets created on a fiber taper. (e) Side view optical image of the microsphere during the coating process. (f) Side view optical image of the microsphere after PDMS coating.

and described in the following. After lithography and hydrofluoric acid etching of silica, a circular silica pad (with a diameter of 100 μm) is formed on the silicon wafer, of which the optical top view image is shown in Fig. 1(a). We then use xenon difluoride gas to etch the underlying silicon to form a supporting silicon pillar under the silica microdisk. In this process, we intentionally reduce the size of the silicon pillars to less than 10 μm in diameter, as shown in Fig. 1(b) (white point). Subsequently, a CO_2 laser is used to reflow the silica microdisk all the way to the pillar to form a silica microsphere (diameter ~30 μm) on a chip, shown in Fig. 1(c). After the fabrication of the silica microsphere, we coat a layer of PDMS (RTV 615, 10:1) onto the cavity surface using the method reported in [11]. For this, PDMS droplets are first created on a fiber taper. The silica microcavity, controlled by a nano-positional stage, then approaches a PDMS microdroplet from underneath. The side view optical images illustrating the coating process are shown in Figs. 1(d)–1(f). In the coating process, the PDMS droplet spreads onto the microsphere from the top to the bottom, which leads to a more uniform coating thickness around the microsphere equator than is achievable with the side-coating technique [11]. In addition, the coating thickness of the PDMS layer is controlled by choosing a droplet with the proper size. After the PDMS droplet has spread uniformly on the silica microsphere surface, a hot plate is used to heat the PDMS-coated microcavity to accelerate the curing process. This coating process can be repeated in order to gradually increase the whole coating thickness of the same microcavity.

To measure the Raman emission spectrum of the PDMS-coated microcavity, a tunable diode laser in the 680 nm wavelength band is used as the excitation light source. Since the refractive index of PDMS (1.41) is very close to that of silica (1.45), a silica fiber taper (with diameter ~400 nm) efficiently couples the light into the microcavity under the phase-matching condition. The transmitted pump light and emitted Raman laser are collected by the same fiber taper and then split into two ports, with one port detected by a photoreceiver, which is monitored by an oscilloscope, and the other connected to an optical spectrum analyzer to measure the Raman emission spectra.

In our experiment, the Raman emission spectra are obtained for different PDMS coating thicknesses, with a constant excitation power of ~2 mW. The spacing of high-Q modes in a microsphere being smaller than the typical Stokes linewidth of one Raman line of PDMS (~20 cm^{-1}) or of silica (~200 cm^{-1}), Raman emission from the microsphere is always on resonance with a high-Q cavity mode and is therefore visible in the output spectrum. The experimental results are shown in Fig. 2, in which four typical Raman emission spectra are given with the PDMS coating thickness gradually increasing. Figure 2(a) shows the Raman spectrum of a pure silica microcavity (coating thickness $t = 0$), from which we can see that six cascaded Stokes lasing lines are generated, due to the ultrahigh Q factor (up to 10^8) and small mode volume ($V_m \sim 150\ \mu m^3$) of the silica microcavity. With an increase of the PDMS coating thickness, the number of silica Stokes lasing lines decreases, as shown in Fig. 2(b), in which only the first-order Raman lasers of

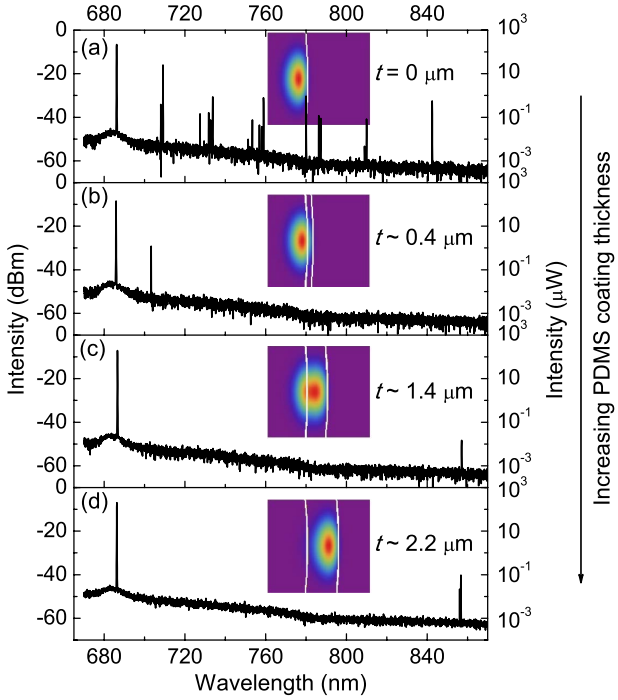

Fig. 2. Raman spectra with an increasing thickness of the coating PDMS layer. The inset images show the corresponding field distributions of the fundamental TE WGM of the PDMS-coated microcavity. The white arcs represent the boundaries of silica and PDMS. Here the thicknesses are estimated from the size of the PDMS droplets used for coating.

silica are observed when $t \sim 0.4$ μm. This is because a small portion of the field energy is distributed in the PDMS layer [with the field distribution shown in the inset of Fig. 2(b)], and the larger absorption loss of PDMS slightly decreases the Q factor of the microcavity. With the thickness of the PDMS coating layer increasing to $t \sim 1.4$ μm, more energy is distributed in PDMS, instead of silica, as shown in the inset of Fig. 2(c). The emission spectrum thus switches from that of silica Raman lasing to that of PDMS Raman lasing, as shown in Fig. 2(c), in which the Raman peak of PDMS at 850 nm wavelength band is observed. With a further increase in the thickness of the PDMS coating layer, almost all the energy is distributed in PDMS [shown in the inset of Fig. 2(d)], and the intensity of the PDMS Raman laser therefore increases, as shown in Fig. 2(d) ($t \sim 2.2$ μm). In this case, the microcavity can be regarded as a pure PDMS microcavity. The Q factor remains over 10^7, corresponding to the value determined by PDMS absorption loss (~0.2 dB/cm) [19].

In order to verify that the laser line around 850 nm does come from stimulated Raman scattering in PDMS, we change the excitation laser wavelength, and measure the Raman spectrum. Figure 3(a) provides four Raman spectra with different excitation laser wavelengths, from which we can see that the Raman laser peak redshifts as the excitation laser moves toward longer wavelengths. The Raman shift stays constant, with a value of ~2900 cm^{-1} [Fig. 3(b)], which corresponds to the strongest fingerprint in the Raman spectrum of bulk PDMS material measured by a Raman spectrometer [Fig 3(c)].

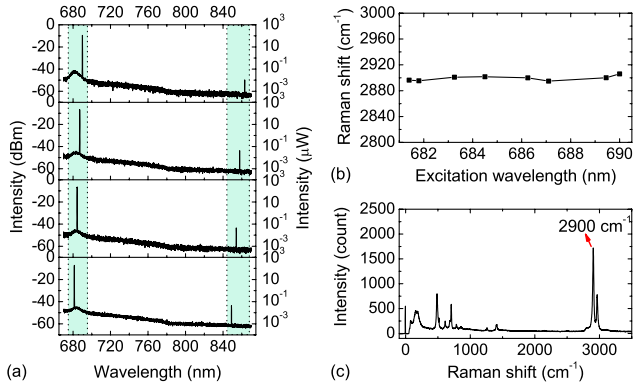

Fig. 3. (a) Four Raman spectra with different excitation laser wavelengths. (b) The experimental PDMS Raman shift versus various excitation wavelengths. (c) The Raman spectrum of bulk PDMS material measured by a Raman spectrometer. In (a), the excitation and Raman lasing wavelength bands are marked with two shadowed rectangles.

Finally, we measure the threshold behavior of the PDMS microcavity Raman laser with a coating thickness of ~2.2 μm, with the results shown in Fig. 4, from which we can see that the threshold of the PDMS microcavity Raman laser is very low, close to 1.3 mW. This threshold is higher than that of the silica microcavity Raman laser. This is due to the larger absorption loss (~0.2 dB/cm) [19] of PDMS, which is responsible for a lower Q factor (~10^7) than that of a pure silica microcavity (10^8).

Since the threshold is inversely proportional to the product of Q_{pump} and Q_{Raman}, it can be lowered by choosing an excitation wavelength for which PDMS has small absorption in both the excitation and Raman lasing wavelength bands. Reducing the microcavity radius R can also lower the Raman lasing threshold, since the threshold is proportional to the mode volume V_m, which is proportional to $R^{1.83}$ [3] for the fundamental mode of a microsphere. Cascaded Raman lasing in PDMS microcavities is also attainable by using a laser with higher power. Furthermore, other polymers with much lower absorption losses in a wide wavelength range can also be chosen, such as poly(methyl methacrylate), which would also lower the threshold of polymer microcavity Raman lasers. In addition, using more sensitive detectors, such as a liquid-nitrogen-cooled-CCD or electron-multiplying-CCD, much weaker Raman signals as low as several femtowatts can be detected. Therefore, specific detection of nanoparticles can be performed by measuring the Raman signals from nanoparticles when bound on the microcavity surface.

In summary, we observe Raman lasing from an on-chip, high-Q PDMS microcavity, created by coating a PDMS layer onto the surface of a silica microsphere, which is to our knowledge the first demonstration of a polymer microcavity Raman laser. This provides a route to creating novel light sources with wavelength bands that are usually difficult to access, and also opens up new possibilities for sensing applications using cavity-enhanced Raman scattering.

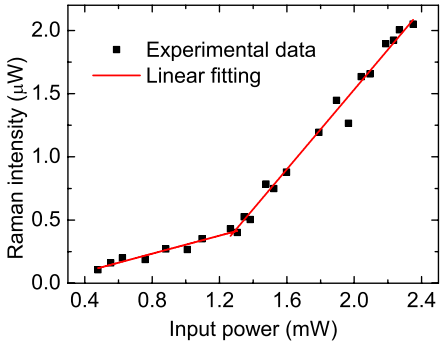

Fig. 4. PDMS Raman laser intensity versus input power.

B. B. Li thanks Xiao-Chong Yu for discussions. This work was supported by the 973 program (grant 2013CB328704), the NSFC (grants 11004003, 11023003, 1121091, and 11222440), the RFDPH (grant 20120001110068), and Beijing Natural Science Foundation Program (grant 4132058). M. Yan Y. was supported by the National Fund for Fostering Talents of Basic Science (grants J1030310 and J1103205).

References

1. H. M. Pask, Prog. Quantum Electron. **27**, 3 (2003).
2. S. M. Spillane, T. J. Kippenberg, and K. J. Vahala, Nature **415**, 621 (2002).
3. T. J. Kippenberg, S. M. Spillane, B. Min, and K. J. Vahala, IEEE J. Sel. Top. Quantum Electron. **10**, 1219 (2004).
4. S.-X. Qian and R. K. Chang, Phys. Rev. Lett. **56**, 926 (1986).
5. H.-B. Lin and A. J. Campillo, Phys. Rev. Lett. **73**, 2440 (1994).
6. H. Rong, S. Xu, O. Cohen, O. Randy, M. Lee, V. Sih, and M. Paniccia, Nat. Photonics **2**, 170 (2008).
7. Z.-P. Liu, Y. Li, Y.-F. Xiao, B.-B. Li, X.-F. Jiang, Y. Qin, X.-B. Feng, H. Yang, and Q. Gong, Appl. Phys. Lett. **97**, 211105 (2010).
8. T. Grossmann, M. Hauser, T. Beck, C. Gohn-Kreuz, M. Karl, H. Kalt, C. Vannahme, and T. Mappes, Appl. Phys. Lett. **96**, 013303 (2010).
9. B.-B. Li, Q.-Y. Wang, Y.-F. Xiao, X.-F. Jiang, Y. Li, L. Xiao, and Q. Gong, Appl. Phys. Lett. **96**, 251109 (2010).
10. R. Madugani, Y. Yang, J. M. Ward, J. D. Riordan, S. Coppola, V. Vespini, S. Grilli, A. Finizio, P. Ferraro, and S. N. Chormaic, Opt. Lett. **37**, 4762 (2012).
11. L. He, Y.-F. Xiao, C. Dong, J. Zhu, V. Gaddam, and L. Yang, Appl. Phys. Lett. **93**, 201102 (2008).
12. Y.-F. Xiao, L. He, J. Zhu, and L. Yang, Appl. Phys. Lett. **94**, 231115 (2009).
13. C.-H. Dong, F.-W. Sun, C.-L. Zou, X.-F. Ren, G.-C. Guo, and Z.-F. Han, Appl. Phys. Lett. **96**, 061106 (2010).
14. H. S. Choi, X. Zhang, and A. M. Armani, Opt. Lett. **35**, 459 (2010).
15. Y. Deng, F. Liu, Z. C. Leseman, and M. Hossein-Zadeh, Opt. Express **21**, 4653 (2013).
16. H. C. Tapalian, J.-P. Laine, and P. A. Lane, IEEE Photon. Technol. Lett. **44**, 1118 (2002).
17. D. K. Armani, T. J. Kippenberg, S. M. Spillane, and K. J. Vahala, Nature **421**, 925 (2003).
18. T. Carmon and K. J. Vahala, Phys. Rev. Lett. **98**, 123901 (2007).
19. S. Kopetz, D. Cai, E. Rabe, and A. Neyer, Int. J. Electron. Commun. **61**, 163 (2007).